Article

pubs.acs.org/Biomac

Poly(methacrylic acid)-Coated Gold Nanoparticles: Functional Platforms for Theranostic Applications

Gokhan Yilmaz,[†,‡,§] Bilal Demir,[∥] Suna Timur,[*,∥] and C. Remzi Becer[*,†]

[†]Polymer Chemistry Laboratory, School of Engineering and Materials Science, Queen Mary, University of London, E1 4NS London, United Kingdom

[‡]Department of Chemistry, University of Warwick, CV4 7AL Coventry, United Kingdom

[§]Department of Basic Sciences, Turkish Military Academy, 06654 Ankara, Turkey

[∥]Faculty of Science, Biochemistry Department, Ege University, 35100-Bornova, Izmir, Turkey

ABSTRACT: The integration of drugs with nanomaterials have received significant interest in the efficient drug delivery systems. Conventional treatments with therapeutically active drugs may cause undesired side effects and, thus, novel strategies to perform these treatments with a combinatorial approach of therapeutic modalities are required. In this study, polymethacrylic acid coated gold nanoparticles (AuNP-PMAA), which were synthesized with reversible addition−fragmentation chain transfer (RAFT) polymerization, were combined with doxorubicin (DOX) as a model anticancer drug by creating a pH-sensitive hydrazone linkage in the presence of cysteine (Cys) and a cross-linker. Drug-AuNP conjugates were characterized via spectrofluorimetry, dynamic light scattering and zeta potential measurements as well as X-ray photoelectron spectroscopy. The particle size of AuNP-PMAA and AuNP-PMAA-Cys-DOX conjugate were calculated as found as 104 and 147 nm, respectively. Further experiments with different pH conditions (pH 5.3 and 7.4) also showed that AuNP-PMAA-Cys-DOX conjugate could release the DOX in a pH-sensitive way. Finally, cell culture applications with human cervix adenocarcinoma cell line (HeLa cells) demonstrated effective therapeutic impact of the final conjugate for both chemotherapy and radiation therapy by comparing free DOX and AuNP-PMAA independently. Moreover, cell imaging study was also an evidence that AuNP-PMAA-Cys-DOX could be a beneficial candidate as a diagnostic agent.

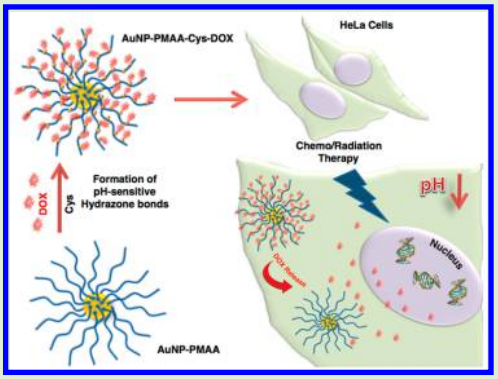

INTRODUCTION

Recently, the use of nanomaterials in drug delivery systems has gained a tremendous attraction in the research of the pharmaceutical industry.[1] Their usage in drug formulations is getting more important due to the limitation by poor penetration of drugs into tumor tissues and adverse effects on healthy cells. Since the conventional therapies, including therapeutically active drug molecule, may not generate a selective distribution for a certain location on the organism, undesirable impacts could have been observed in organs and healthy tissues. In order to prevent side effects, surface modification strategies become crucial because the attachment of targeting moieties to the drug carrier system makes it selective to the target tissue or cells.[2,3] There are two strategies for obtaining the targeted drug delivery: (i) passive targeting and (ii) active targeting. Passive targeting includes the transport of the nanocarriers, though leaky vasculature of the diseased tissues via convection or passive diffusion and this technique reveals the enhanced permeability and retention (EPR) effect of the drug carrier systems.[4,5] The use of passive targeting may cause the accumulation of the nanocarriers within long circulation time in solid tumors.[6] For being the appropriate candidate to use in passive targeting with EPR effect, the nanocarriers should include three important properties; first, they should be larger than 10 nm to avoid the filtration by the kidneys and should be about 100 nm to avoid the specific capture by the liver; second, the nanocarriers should be nonionic or anionic in order to avoid the renal elimination; and third, they should be recognized by the reticuloendothelial system for not to be phagocytosed.[7] Within this strategy, many drug delivery systems have been reported, especially with the use of metallic nanoparticles, polymers, lipid, or surfactant-based vesicular carriers.[8−12] Active targeting of nanoparticles contains peripherally conjugated targeting ligands for enhanced and selective delivery. The targeting ligands such as antibodies, folic acid, glycoconjugates, or nucleic acids like aptamers are important to the mechanism of cellular uptake. Long circulation times will allow for effective transport of the nanoparticles to the tumor site through the EPR effect, and the targeting molecule is able to increase endocytosis of the nanoparticles. The internalization of nanoparticle drug delivery systems has shown an increased therapeutic effect.[13,14]

Those drug delivery systems have been generally constructed for the cancer treatment which remains the major common

Received: May 16, 2016
Revised: July 20, 2016
Published: July 22, 2016

DOI: 10.1021/acs.biomac.6b00706
Biomacromolecules 2016, 17, 2901−2911

cause of morbidity and mortality throughout the world.[15] In the treatment of cancers, a combination of several types of therapeutic modalities with distinct mechanisms is considered to be a potential strategy.[16] Chemotherapy is one of the most common therapies employed in oncology. Therefore, newly designed drug delivery systems are regarded as a new paradigm in cancer chemotherapy, particularly by creating pH-sensitive infrastructures thanks to the feature of lower acidic matrix of cancerous tissue.[17] By using this prominent information, numerous chemotherapeutic strategies were developed involving a pH-dependent conjugation approach.[18−20] Concomitantly, novel multifunctional carriers also offer combinatorial therapies with this approach. In a related study, Chen et al. designed a novel kind of intelligent nanogels that can spatiotemporally control the release of doxorubicin and photosensitizers to combine chemotherapy and photodynamic therapy.[21]

Gold nanoparticles (AuNPs) are emerging as an efficient platform for diagnostic and therapeutic purposes since they have several unique features such as chemical inertness, facile surface functionalizability, and electronic structure amenable for plasmon resonance and optical properties suitable as imaging agents.[22] On the other hand, in spite of the synthesis of AuNPs is well-advanced, sometimes colloidal stability of NPs might create aggregation problems in the case of long-term stability. Furthermore, AuNPs are known as nontoxic, however, AuNPs with the size of 1.4 nm induced the toxicity of HeLa cells to a greater extent rather than 15 nm AuNPs.[23] Meanwhile, toxicity of colloidal NPs is also due to the surface chemistry. In regard to this situation, it has to be essential to control precisely the functional groups on the surface as well as remove residual contaminants, especially citrate, arising from the particle synthesis.[24−26] Therefore, polymer-covered AuNPs are considerably in importance under favor of contribution of expanded functionalities, composition and charge. To date, several studies were reported the AuNPs covered with polyethylene glycol (PEG),[27] hyaluronic acid,[28] chitosan,[29] thiolated polyvinylpyrrolidone,[30] heparin,[31] and so on. Additionally, AuNPs have an excellent capability in the radiation therapy. Radiotherapy, which is known as another commonly used therapeutic tool for the treatment of half of the cancers is based on the cancer tissue damage with the generation of reactive oxygen species (ROS) like hydroxyl radical (OH^-) and superoxide anion (O^{2-}) upon illumination with X-rays. Beside, gold (atomic number, $Z = 79$) has a better radiation effect than other radiosensitive elements such as carbon ($Z = 6$), gadolinium ($Z = 64$), and platinum ($Z = 78$) due to the photoelectric effect of gold.[32] Also, PEG, polysaccharides, poloxamines, or poloxamers covered AuNPs were introduced to radiation therapy.[33]

Herein, a combined nanoplatform involving both polymethacrylic acid coated AuNPs (AuNP-PMAA) and an anticancer drug doxorubicin (DOX) was synthesized with a pH-sensitive hydrazone linkage between cysteine (Cys) modified AuNP-PMAA and DOX. Following the successful preparation of DOX conjugated AuNP, which was denoted as "AuNP-PMAA-Cys-DOX", spectroscopic and physicochemical characterizations and in vitro drug release studies were accomplished. AuNP-PMAA-Cys-DOX conjugates were applied for the further cell culture studies, including cytotoxicity, radiotherapy, and cell imaging, by using Human cervix adenocarcinoma cell line (HeLa). To evaluate the effectiveness of AuNP-PMAA-Cys-DOX platforms, AuNP-PMAA and free DOX were tested for the comprehensive comparison.

EXPERIMENTAL SECTION

Reagents. Methacrylic acid (MAA, 99%, contains 250 ppm monomethyl ether hydroquinone (MEHQ) as inhibitor), 2-Cyano-2-propyl benzodithioate (CPBDT, 97%), sodium borohydride ($NaBH_4$, 98%, granular, 10−40 mesh), and gold nanoparticle suspension (40 nm) that stabilized with citrate were purchased from Sigma-Aldrich Chemical Co. (Dorset, U.K.). MAA was passed through a short column of basic alumina in order to remove MEHQ inhibitor prior to polymerization. 4,4′-Azobis(2-methylpropionitrile) (AIBN) was previously synthesized within the group. All other reagents and solvents were obtained at the highest purity available from Sigma-Aldrich Chemical Co. (Dorset, U.K.) and used as received unless stated otherwise. Water (H_2O, HiPerSolv Chromanorm for HPLC from VWR International, U.K.) was used throughout the study. Dialysis tubes were purchased from Spectrum Laboratories (California, U.S.A.). Copper-coated 3.05 mm diameter square carbon film mesh grids were purchased from Agar Scientific (Essex, U.K.). Doxorubicin (DOX), Cysteine (Cys), *N*-(3- dimethylaminopropyl)-*N*′-ethylcarbodiimide hydrochloride (EDC), *N*-hydroxysuccinimide (NHS), 3-(4,5-dimethylthiazolyl-2)-2,5-diphenyltetrazolium bromide (MTT), and sodium dodecyl sulfate (SDS) were obtained from Sigma-Aldrich (St. Louis, U.S.A.). *N*-ε-Maleimidocaproic acid hydrazide (EMCH) was obtained from Thermo Fischer Scientific (California, U.S.A.). Dulbecco's Modified Eagle Medium (DMEM), penicillin/streptomycin (10000 UI/mL), L-glutamine (200 mM), trypsin/EDTA (0.05% trypsin; 0.2 g/L EDTA), and phosphate buffered saline (PBS) used in cell culture experiments were obtained from Lonza (Basel, Switzerland). Fetal bovine serum (FBS) was purchased from Biowest (Nuaillé, France).

Synthesis of Poly(methacrylic acid) (PMAA). RAFT polymerization of MAA was carried out in the presence of CPDBT as a RAFT agent, AIBN as an initiator in the methanol and water mixture (2:1) at 70 °C for 12 h. A Schlenk tube was charged with MAA monomer (100 equiv), CPDBT (1 eg), AIBN (0.1 eg), and the solvent (3.0 mL) was degassed by gentle bubbling of argon gas for 30 min. The Schlenk tube was sealed properly, and the mixed solution was allowed to polymerize. After the confirmation of >98% conversion according to gas chromatography (GC), the polymerization reaction was stopped by cooling down and exposure to the air. Subsequently, the reaction solution was diluted with 3.0 mL of tetrahydrofuran (THF) and then purified by precipitation in diethyl ether. After the filtration, the obtained polymer was dried in vacuo and characterized via ^{1}H NMR and *N*,*N*-dimethylformamide (DMF) SEC analysis.

Reduction of the RAFT End Group of PMAA. The RAFT end group of the obtained polymer was reduced by the addition of $NaBH_4$ as the reducing agent in the distilled water. PMAA homopolymer was added into a 50 mL round-bottom flask with 10 mL of water solution of 1.0 M $NaBH_4$, and the solution was bubbled for 15 min (molar ratio of $NaBH_4$/dithioester end groups was 25:1). After that, the mixture was allowed to react for 2 h. Following reduction, the homopolymer solution was dialyzed against water for 3 days, while changing the water at least three times. Finally, it was freeze-dried to get the polymer with thiol end group. The product was characterized by ^{1}H NMR and DMF SEC analysis.

Preparation of PMAA-Substituted AuNPs. The AuNPs solution was centrifuged in order to remove the supernatant and then replaced by the same volume of water prior to the PMAA functionalization. Terminally thiolated poly(MAA) (10 mg) was dissolved in 1.0 mL of AuNP solution and then agitated in the dark for overnight. To remove excess polymer, the solution of the AuNP-stabilized PMAA were centrifuged (5470 rpm, 30 min). Following careful decantation of the supernatant, the nanoparticles were then redispersed in 1.0 mL of deionized water, and then the centrifugation and resuspension process was repeated one more cycle. These synthesized PMAA-substituted GNPs were characterized by dynamic light scattering (DLS), UV/vis spectroscopy, thermogravimetric analysis (TGA), and transmission electron microscopy (TEM). The PMAA-coated AuNPs were stored at 4 °C for the further study. The general scheme of the reactions

DOI: 10.1021/acs.biomac.6b00706
Biomacromolecules 2016, 17, 2901−2911

Scheme 1. RAFT Polymerization of MAA and Formation of PMAA-Stabilized AuNPs

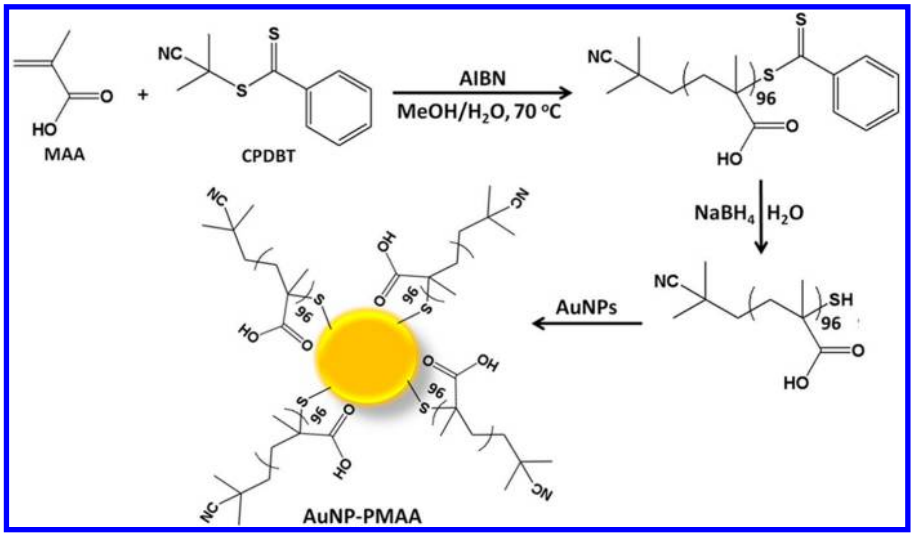

Scheme 2. Conjugation Reactions of the AuNP-PMAA-Cys-DOX Particles

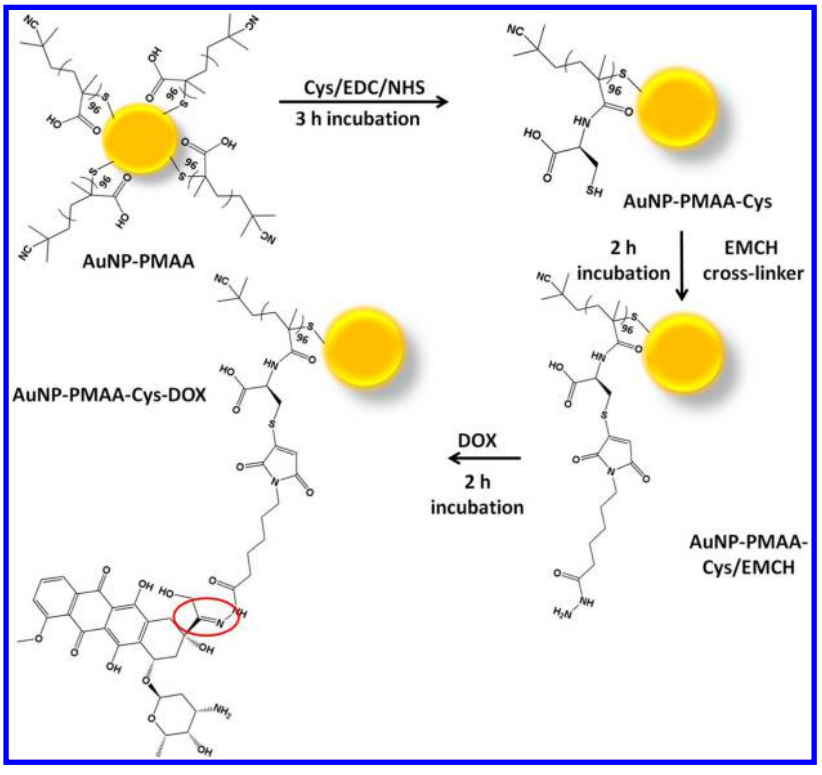

related to the synthesis of PMAA covered AuNPs was given in Scheme 1.

Construction of pH-Sensitive AuNP-PMAA-Cys-DOX Bioconjugate. The bioconjugation of polymer capped AuNPs is carried out as three main steps. Initially, AuNPs that have pendant carboxylic acid (−COOH) groups via PMAA structure were activated with EDC/NHS chemistry, and covalent amide bonds were generated by adding Cys. For this purpose, the mixture of 25 μL of PMAA-AuNP (100 mg/mL dissolved in 10 mM phosphate buffer, pH 7.4), 48.9 mg EDC, 7.2 mg NHS, and 250 μL of Cys (from 1.0 mg/mL stock solution dissolved in pH 5.0 MES buffer) was prepared (V_{total} = 1500 μL with the addition of MES buffer) and incubated for 3 h with 1000 rpm shaking under ambient conditions. After the incubation step, a final mixture was dialyzed against pH 7.4 PBS for 2 h. The dialyzed bioconjugate solution was treated with DTT (1:0.9 molar ratio of Cys/DTT). This mixture was incubated overnight under 1000 rpm shaking and ambient conditions. After the reduction of S−S linkages between Cys residues, EMCH cross-linker was added as 3.2 mg and reacted for 2 h at 1000 rpm shaking at room temperature. After incubation, the mixture was dialyzed for 6 h against PBS pH 7.4. In the final step, DOX (50 μM as the final concentration) was added to the AuNP-PMAA-Cys (EMCH) solution and incubated for 2 h at 1000 rpm shaking and room temperature and final solution was increased to 2.0 mL. The final AuNP-PMAA-Cys-DOX conjugate was dialyzed overnight against PBS, pH 7.4. The conjugation steps for the formation of pH-sensitive hydrazone linkage in AuNP-PMAA-Cys-DOX were given in Scheme 2.

CHARACTERIZATION

^{1}H NMR spectroscopy (Bruker DPX-400) was used to determine the chemical structure of the synthesized polymers.

DOI: 10.1021/acs.biomac.6b00706
Biomacromolecules 2016, 17, 2901−2911

Samples were dissolved at 10 mg/mL concentration in D_2O or DMSO, depending on the solubility of the samples.

Size-exclusion chromatography (SEC) measurements were conducted on an Agilent 1260 infinity system operating in DMF with 5.0 mM NH_4BF_4 and equipped with refractive index detector (RID) and variable wavelength detector (VWD), two PLgel 5 μm mixed-C columns (300 × 7.5 mm), a PLgel 5 mm guard column (50 × 7.5 mm), and an autosampler. The instrument was calibrated with linear narrow poly(methyl methacrylate) standards in the range of 550−46890 g/mol. All samples were passed through 0.2 μm PTFE filter before analysis.

Gas chromatography (GC) was used to monitor the monomer conversion for homopolymerization of MAA. GC analysis was performed using an Agilent Technologies 7820A. An Agilent J&W HP-5 capillary column of 30 m × 0.320 mm with a film thickness of 0.25 mm was used. The oven temperature was programmed as follows: 40 °C (hold for 1 min) increase at 30 °C/min to 300 °C (hold for 2.5 min). The injector was operated at 250 °C and the FID was operated at 320 °C. Nitrogen was used as carrier gas at a flow rate of 6.5 mL/min, and a split ratio of 1:1 was applied. Chromatographic data was processed using OpenLab CDS ChemStation Edition, version C.01.05.

Thermal gravimetric analysis (TGA) was conducted with a TA Instruments TGA Q500 under a nitrogen atmosphere using approximately 5.0 mg of the respective sample for the analysis. Method settings: heating from 100 to 900 °C with a heating rate of 10 °C/min. UV measurements were performed on a PerkinElmer UV/vis Spectrometer Lambda 35.

Transmission electron microscopy (TEM) analysis was carried out on a JEOL 1400 instrument operating at an acceleration voltage 200 kV. The TEM specimens were made by placing a drop of a nanoparticle water suspension on a carbon-coated copper grid.

Spectrofluorimetric and X-ray photoelectron spectroscopy (XPS) analysis were carried out to confirm the conjugation of AuNP-PMAA particles to DOX, particle size, and surface charge. Size distribution and zeta potential of AuNP-PMAA-Cys-DOX conjugates were measured by a dynamic light scattering (DLS) method with Zetasizer Nano ZS (Malvern Instruments Ltd., U.K.) at a scattering angle of 90° using a wavelength of 633 nm and at 25 °C. Prior to measurements, the samples (50 μL) were diluted to 1.0 mL with PBS, and each sample was measured three times. Zeta potential of samples was calculated by the device according to Smoluchowski equation. The samples were kept in +4 °C when not in use. Fluorimetric and spectroscopic properties of AuNP-PMAA-Cys-DOX were assessed via a Varioskan spectrofluorometer (Thermo, Fischer, U.S.A.). XPS analysis (PHI 5000 VersaProbe, Minnesota, U.S.A.) of the final drug-AuNP conjugate was accomplished, too. Prior to measurements, AuNP-PMAA-Cys-DOX solution was dried over an ultrasonically cleaned indium tin oxide surface.

In Vitro Drug Release. The in vitro release behavior of DOX-loaded nanoparticles was monitored by creating artificial media. pH values of 7.4 and 5.3 (PBS) were used to simulate the healthy and cancerous cellular environments, respectively. Dialysis bags containing 0.5 mL of sample were submerged in 5.0 mL of buffer medium at 37 °C at 100 rpm. To investigate the in vitro release profiles of the samples, 0.5 mL of each of the samples was collected at several time intervals (0 and 30 min and 1, 2, 4, 6, 8, 12, 24, 48, and 72 h) and replaced with an equal volume of fresh medium.

The concentration of DOX in the collected samples was determined by fluorescence spectroscopy using a standard curve that was generated by the fluorescence properties of DOX. Probing the released DOX, the cumulative drug release percentage (E_r) was calculated according to the following equation:

$$E_r = \frac{V_e \sum_1^{n-1} C_i + V_o C_n}{M(\mathrm{Dox})}$$

where M(Dox) represents the amount of DOX in the particles, V_o is the whole volume of the release media (V_o = 5.0 mL), V_e is the volume of the replace media (V_e = 0.5 mL), and C_n represents the concentration of DOX in the nth sample.

Cell Culture Studies. Human cervix adenocarcinoma cell line (HeLa; American Type Culture Collection) was maintained in DMEM supplemented with 10% FBS, 100 UI/mL penicillin/streptomycin, and 2.0 mM, L-glutamine at 37 °C in a humidified incubator with 5.0% CO_2. HeLa cells were subcultured at 80% confluency. Following the synthesis of AuNP-PMAA-Cys-DOX bioconjugate, cell culture studies, including toxicity, cell imaging, and radiosensitivity with HeLa cells.

Cytotoxicity. A cell proliferation assay kit (MTT reagent) was used to determine the changes in cell viability of cells treated with samples. To perform the MTT assay, HeLa cells were seeded into 96-well plates and incubated until reaching confluence with normal morphology. The samples of AuNP-PMAA, DOX, and AuNP-PMAA-Cys-DOX with varying concentrations were added to wells and then the cell culture plates were placed in a CO_2 incubator for incubation at 37 °C for 2 h. After incubation, the cells were washed to remove culture medium. MTT assay on the cell lines was carried out according to standard procedure. The dose-dependent cell viability of bioconjugates was reported as cell viabilities relative to the control (untreated) cells.

Cell Imaging. In order to observe the interactions of the constructed AuNP-PMAA-Cys-DOX bioconjugates and free DOX with HeLa cells, 100 μL of samples were introduced into the cells grown in a chamber slide for 2 days. The cell images were taken by a fluorescence microscope (Olympus BX53F) equipped with a CCD camera (Olympus DP72). Following the treatment for 2 h at 37 °C in CO_2 incubator, the cells were rinsed twice with PBS. Cell images were given by merging with phase-contrast images of cells and fluorimetric images of free DOX and bioconjugates.

Radioactivity. In the radiotherapy study, HeLa cells were treated with commercial AuNP (40 nm), AuNP-PMAA, free DOX, and AuNP-PMAA-Cys-DOX for 24 h, followed by irradiation with 2.5, 5.0, and 10 Gray (Gy) using a 6 MV linear accelerator system (LINAC, Siemens Primus, Germany). A total of 4000 cells/well were incubated at 96-well cell culture plate for 24 h under standard culture conditions. Then, medium was removed and AuNP, AuNP-PMAA, AuNP-PMAA-Cys-DOX (250 μg/mL and the equivalent of 5.0 μM DOX for the final conjugate), and free DOX (5.0 μM) were applied for 2 h. A control group was added with no sample treatment for the comparison. After radiation treatment, cells were incubated for 72 h and cell viability was assessed via the MTT method described above.

DOI: 10.1021/acs.biomac.6b00706
Biomacromolecules 2016, 17, 2901−2911

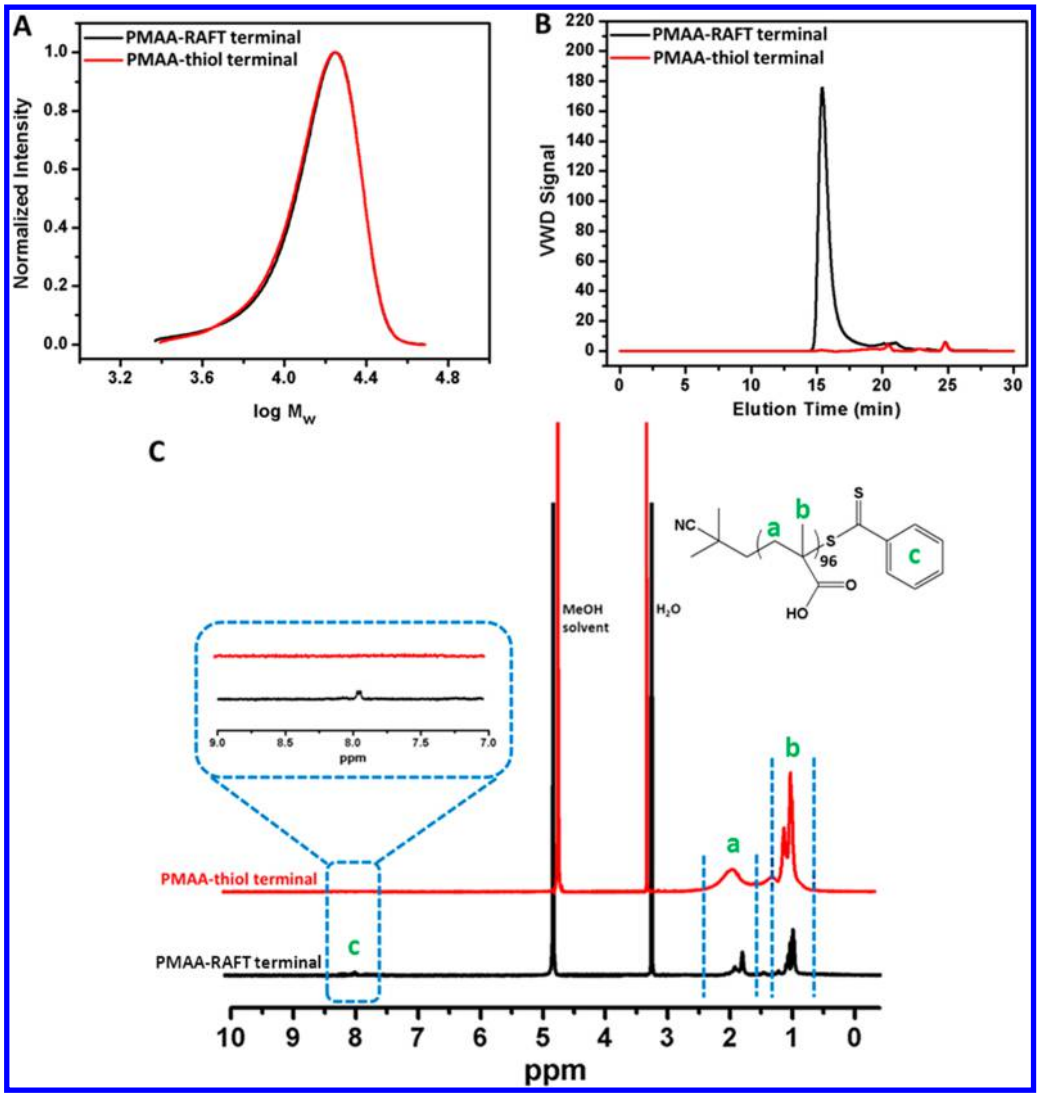

Figure 1. (A) SEC analysis via RI detector and (B) via VWD; (C) ^{1}H NMR characterization of the synthesized PMAA homopolymer before and after the reduction of the RAFT terminal group.

Statistical Analysis. Statistical analyses were conducted using GraphPad Prism software (GraphPad Software, La Jolla, CA, U.S.A.). Data were evaluated using one-way analysis of variance with Tukey's multiple comparison post-test. Comparisons with $p < 0.05$, $p < 0.01$, and $p < 0.001$ were considered as statistically significant.

RESULTS AND DISCUSSION

Synthesis of AuNP-PMAA. The homopolymerization of MAA has been achieved with a good control due to a narrow polydispersity index with high molecular weight via RAFT polymerization. The polymerization reaction was performed in methanol/water at 70 °C for 12 h. After the purification, DMF SEC analysis based on PMMA standards revealed a single peak with an apparent M_n = 12.1 kg/mol and M_w/M_n = 1.18 (Figure 1). The polymerization conversion was calculated using GC and ^{1}H NMR by comparing the integrated signal intensity due to the aromatic hydrogen atoms of the RAFT agent at 7.8−7.9 ppm with that due the vinylic protons of MAA at 5.8−6.2 ppm. Both characterizations revealed that conversion reached ≈96%. A small amount of tailing was detected in according to SEC analysis. The possible reason for that could be an interaction of carbocyclic acid moieties of the homopolymer and SEC column packed materials. Moreover, the M_n by SEC is slightly higher than the theoretical molecular weight mainly due to the different structure of PMAA with PMMA calibration standard and tailing. The theoretical number-average molecular weight, $M_{n(Theo)}$, was calculated as 8.5 kDa by using ($M_{n(Theo)}$ = ([M]$_0$/[RAFT]$_0$ × conversion × M_{MAA}) + M_{RAFT} equation, where [RAFT]$_0$ is the initial RAFT concentration, [M]$_0$ is the initial monomer concentration, M_{MAA} is the monomer molecular weight, and M_{RAFT} is the RAFT agent molecular weight.

Reduction of the RAFT End Group of PMAA. The RAFT agent terminal group of PMAA was reduced to thiol-terminal one in order to immobilize PMAA onto gold nanoparticles in the presence of aqueous $NaBH_4$. ^{1}H NMR and SEC were used to analyze the homopolymer before and after the reduction.

The disappearance of the aromatic protons of the RAFT agent at 7.8−7.9 ppm after being treated indicated that all end groups in the CPDB units have been reduced. As depicted in Figure 1, no obvious change in the SEC traces was observed and the molecular weight was similar to that of before treatment in according to RI detector of SEC. However,

DOI: 10.1021/acs.biomac.6b00706
Biomacromolecules 2016, 17, 2901−2911

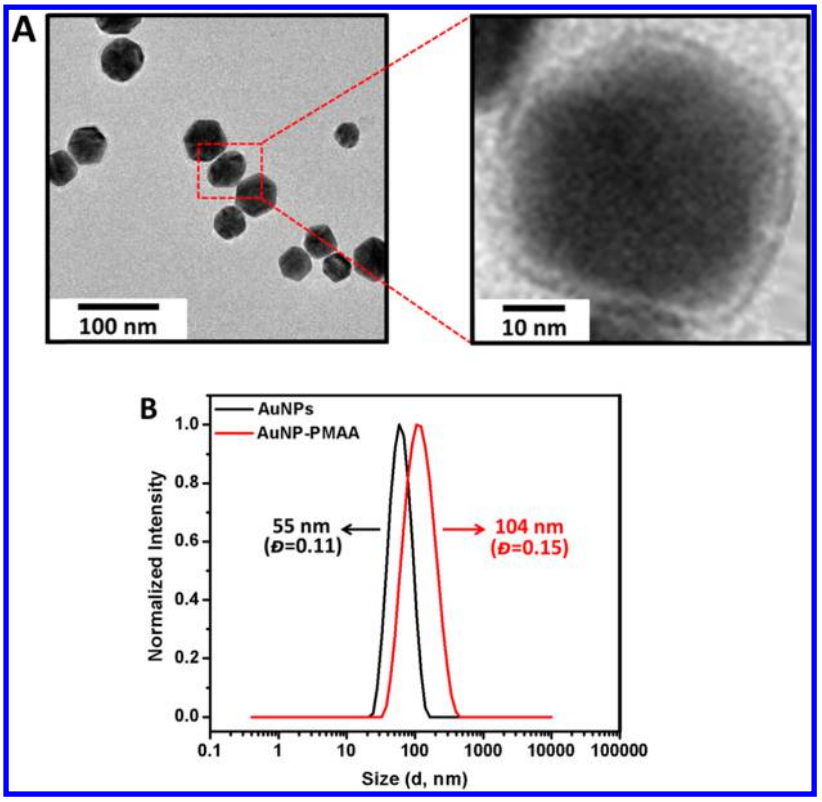

Figure 2. TEM images of the obtained PMAA-coated AuNP and DLS measurement of AuNPs and PMAA-coated AuNP.

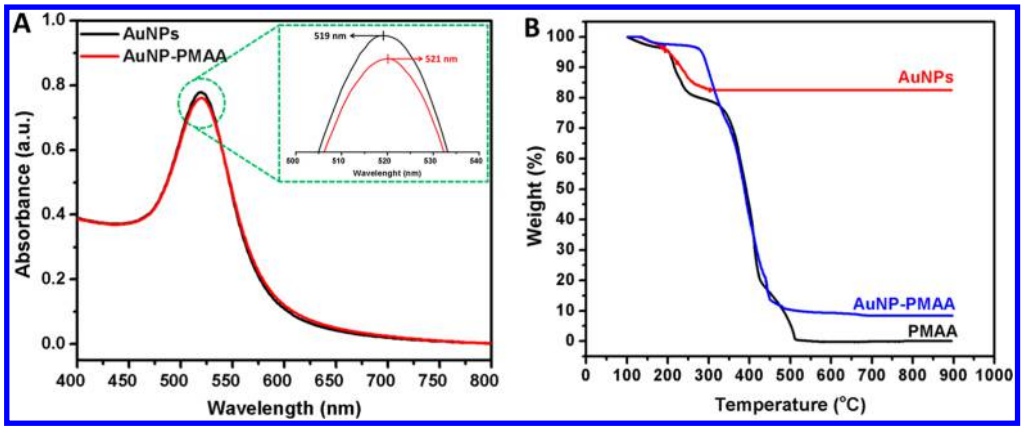

Figure 3. UV/vis spectroscopy characterization of AuNPs and PMAA-coated AuNP and TGA measurements of AuNPs, PMAA, and PMAA-coated AuNP, respectively.

Variable Wavelength Detector (VWD) of SEC at 308 nm did not show any significant peak after treatment (Figure 1) indicating that the PMAA-SH chains were successfully obtained. In contrast, an intense UV signal associated with PMAA-RAFT terminal polymer elution was observed.

Preparation of PMAA-Substituted GNPs. Prior to the PMAA functionalization, the AuNPs solution was centrifuged. The supernatant was removed and replaced by the same volume of water. Then, PMAA-coated gold nanoparticles were prepared by mixing PMAA and AuNPs in the dark for overnight. First, the obtained PMAA-coated AuNPs were characterized via DLS and UV/vis spectroscopy in terms of the investigation of the size and surface plasmon resonance maximum band (SPR_{max}) value change. The SPR_{max} band of AuNPs is usually in accordance to the nanoparticle size, shape, aggregation, and also their dielectric environment. As seen in Figure 3, the position of the SPR_{max} band shifted from 519 to 521 nm due to adsorption of PMAA on the surface. Moreover, UV absorbance peak confirmed that the AuNPs coated with thiol-terminated PMAA were still spherical in shape and also did not show any aggregation due to not any large broad shift in the UV absorbance.

PMAA-substituted GNPs were characterized in terms of the size and zeta potential by using DLS. There was a significant increase in the hydrodynamic volume between AuNPs and PMAA-AuNP, indicating successful immobilization of PMAA onto the surface. As depicted in Figure 2, the size of the gold nanoparticles after the coating with PMAA increased from 55.7 ± 0.2 nm to 104 ± 0.7 nm with polydispersity index (PDI) as 0.15, signifying a narrow particle size distribution. Moreover, the magnitude of the negative zeta potential increased from −26.9 ± 0.2 to −43.6 ± 0.8 mV due to the deprotonation of

DOI: 10.1021/acs.biomac.6b00706
Biomacromolecules 2016, 17, 2901−2911

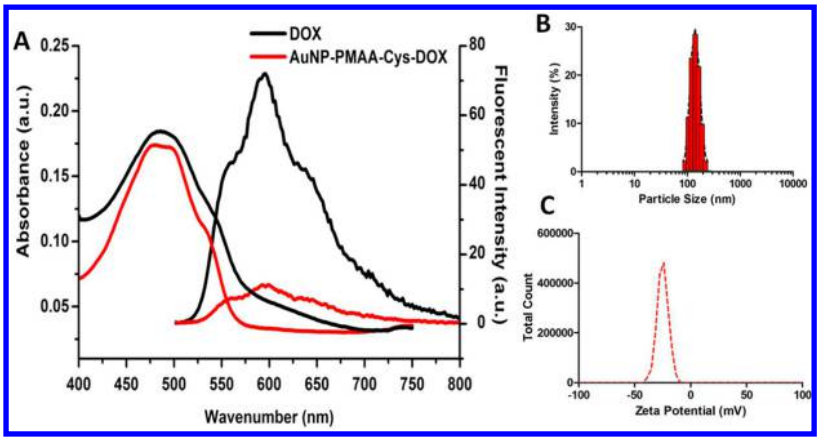

Figure 4. (A) Spectrophotometric characterization of 1.25 mg/mL AuNP-PMAA-Cys-DOX bioconjugate (red lines; containing 25 μM DOX) and 25 μM free DOX (black lines); (B) Particle size and (C) zeta potential analysis of AuNP-PMAA-Cys-DOX.

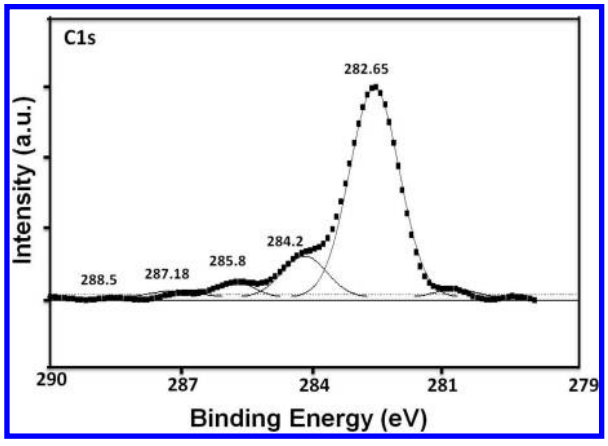

Figure 5. XPS scan of C 1s of AuNP-PMAA-Cys-DOX conjugation.

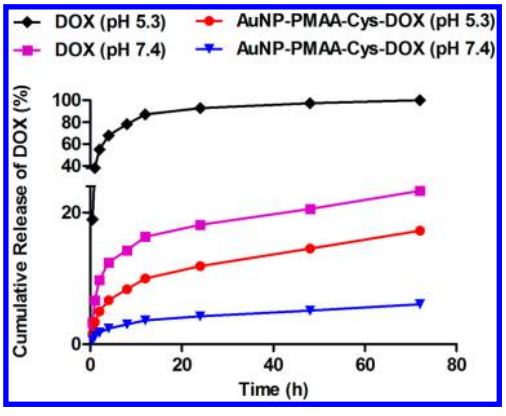

Figure 6. Cumulative drug release profiles of free DOX at pH 7.4 and AuNP-PMAA-Cys-DOX bioconjugates at pH 5.3 and pH 7.4 for 72 h at 37 °C.

the carboxyl group (RCOOH ↔ $RCOO^- + H^+$) in aqueous solution. According to TEM images, the size of PMAA-coated gold nanoparticles ranged between 52 ± 1.4 and 65 ± 2.6 nm. The average size of the monodisperse nanoparticles was calculated as 57 ± 1.8 nm.

In order to determine the amount of the PMAA polymer immobilized onto AuNPs, TGA was performed to analyze each materials thermal profile. As seen in Figure 3, PMAA-coated AuNP exhibited mass loss until approximately 650 °C due to the decomposition of the PMAA polymer onto the surface, and the remaining fraction was the Au core of the synthesized nanoparticles that was unaffected at temperature as high as 650 °C. It was observed that PMAA substituted AuNPs contained 87.4% of the polymer.

Synthesis and Characterization of AuNP-PMAA-Cys-DOX. Following the successful synthesis of polymethacrylic acid coated AuNPs, a covalent binding strategy between AuNP-PMAA and Cys via EDC/NHS chemistry was applied to create a host structure for constructing a pH-sensitive bond between AuNP-PMAA-Cys and DOX in PBS and under ambient conditions.

As the initial characterization step of AuNP-PMAA-Cys-DOX conjugate, the spectrophotometric properties were investigated. The fluorescence and UV−vis spectra of conjugate were illustrated in Figure 4. To compare the spectral features of DOX before and after conjugation procedure, free DOX was also used at the same concentration in AuNP-PMAA-Cys-DOX conjugate. As revealed in Figure 4A, DOX could show its fluorescence emission at 600 nm (ex: 480 nm) while it was conjugated to AuNP-PMAA-Cys. Herein, the DOX conjugation was proved with the decrease of fluorescence intensity and absorption peaks, which was caused by the conjugation steps. In the other studies, similar cases showed up as demonstrated in Du et al.[34] and Shantni et al.[35] by conjugation of polymer-quantum dots and PEGylated palladium nanoparticles. However, DOX could protect its spectral properties in the visible area, thereby this issue could be beneficial in calculating the binding efficiency (BE %) of DOX to AuNP-PMAA particles. Hence, a standard curve was generated in the concentration range of 2.5−100 μM DOX with an equation of $y = 0.0068x + 0.012$ ($R^2 = 0.999$) by reading the absorbance at 480 nm. Then, the freshly synthesized 1.25 mg/mL AuNP-PMAA-Cys-DOX conjugate was measured, and the repeatable results showed that Cys extended and polymer-coated AuNPs could bind 25.5 μM of DOX. Therefore, the BE was calculated as 51% by using the following formula:

$$\text{BE\%} = (\text{DOX concn in conjugate/total DOX concn}) \times 100$$

After the spectroscopic characterization of AuNP-PMAA-Cys-DOX conjugate, another physicochemical parameter was investigated in terms of particle size and zeta potential (Figure 4B,C). The hydrodynamic particle sizes of AuNP-PMAA and AuNP-PMAA-Cys-DOX were assessed as 104 ± 0.7 nm (polydispersity index (PDI): 0.15) and 147 ± 25 nm (PDI: 0.43), respectively. According to the subsequent zeta potential

DOI: 10.1021/acs.biomac.6b00706
Biomacromolecules 2016, 17, 2901−2911

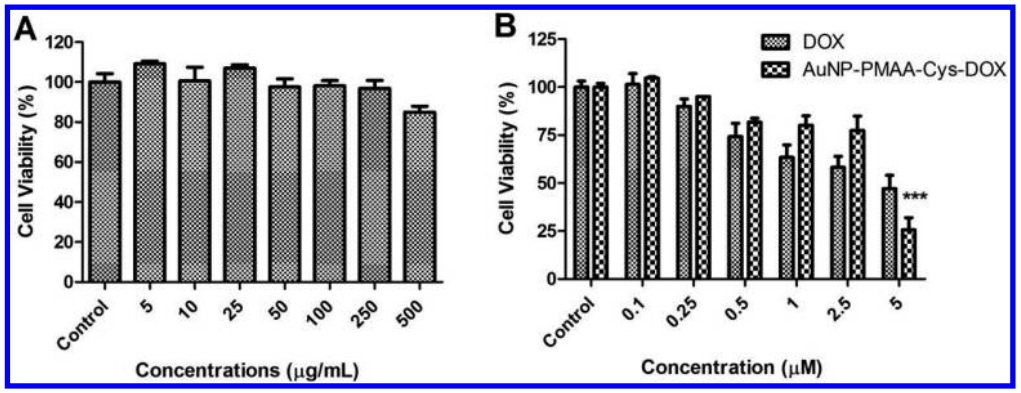

Figure 7. Dose-dependent toxicity of AuNP-PMAA (A), AuNP-PMAA-Cys-DOX and free DOX (B) for HeLa cells. Error bars mean ± standard deviation (n = 4).

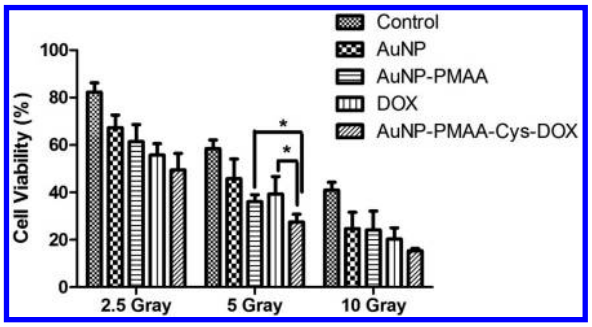

Figure 8. Radiosensitivity effect of uncoated AuNP, AuNP-PMAA, free DOX, and AuNP-PMAA-Cys-DOX at different ionizing radiations (2.5, 5.0, and 10 Grays).

analysis, the surface charges of AuNP-PMAA and AuNP-PMAA-Cys-DOX were assessed as −43.6 ± 0.8 and −22.7 ± 12 mV, respectively. Expectedly, the hydrodynamic particle size of AuNP-PMAA was increased after the DOX conjugation. Moreover, the negative surface charge formed from the −COOH side groups of PMAA was decreased by covering the surface with Cys and DOX. It is known that negatively surface charged NPs demonstrate a reduced plasma protein adsorption and low rate of nonspecific cellular uptake.[36,37] Additionally, the charged NPs can repel one another to overcome the natural tendency of aggregation of NPs.[38] Hence, it can be claimed that newly synthesized AuNP-PMAA and their DOX conjugated forms could be suitable for the accumulation in the cancerous tissue by EPR effect thanks to their good dispersion stability, which was supported by PDI values.

In addition to the physicochemical parameters, XPS of the AuNP-PMAA-Cys-DOX was employed to observe the demand typical bonds of the final conjugate via the binding energies. XPS spectrum in Figure 5 illustrates the detailed information about the crucial bonds, which were used in the conjugation

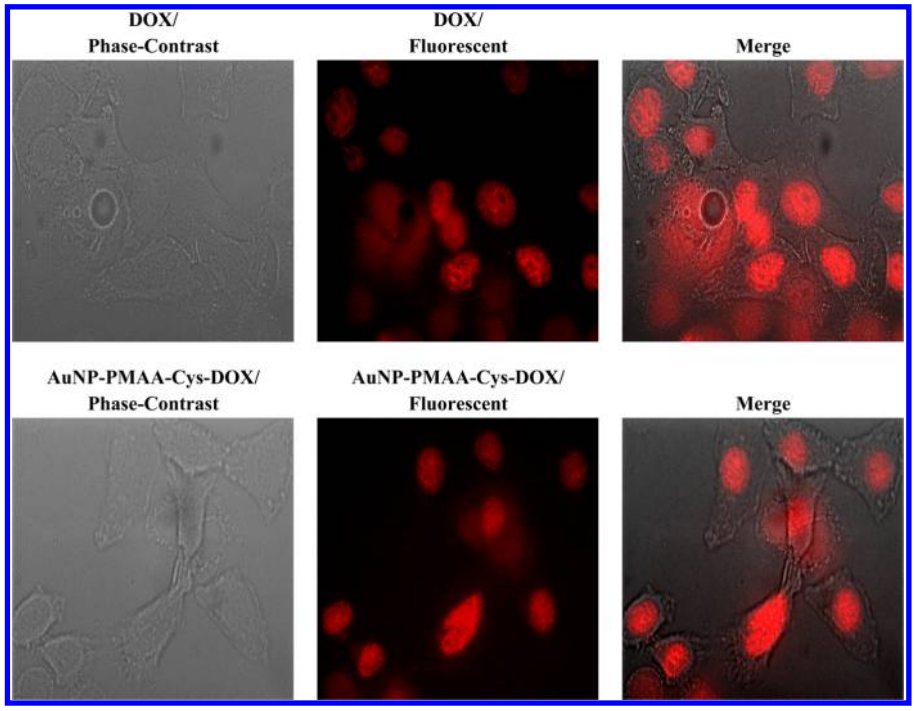

Figure 9. Imaging of HeLa cells with phase-contrast and fluorescence technique. Images were obtained after treatment of the cell with free DOX and AuNP-PMAA-Cys-DOX conjugate for 2 h at 37 °C and 5.0% CO_2 atmosphere, under humidity. Images of samples were taken with a red filter of fluorescence set up with 100× magnification.

DOI: 10.1021/acs.biomac.6b00706
Biomacromolecules 2016, 17, 2901−2911

steps, including an amide bond between carboxyl residues of AuNP-PMAA and amino group of Cys and hydrazone as the pH-sensitive linkage. In the spectra, the binding energy of 282.65 eV reveals the typical C−C bonds. Normally, C−C binding energy shows itself approximately 284 eV.[39,40] However, it was proved that chemisorption of carbon over a surface could show its binding energy at 282.6 eV.[41] In addition, amide bond of O═C−N reveals itself at 287.18 eV with a shift and binding energy of 285.8 presents the typical hydrazone linkage (C═N) as detected in previous studies.[42,43] Furthermore, a small shoulder at 288.5 eV of binding energy shows the RCOO− groups, which might come from the Cys residues or nonconjugated carboxyl group over PMAA.[44]

In Vitro Drug Release. In addition to the characterization steps, in vitro release profiles of DOX-conjugated, polymer-coated AuNPs were generated in order to investigate the potential use of these particles as delivery carriers. One of the main characteristic feature of tumor sites is that having the slightly acidic microenvironment.[45] Therefore, the current study was aimed to generate a pH-sensitive DOX conjugation using the AuNP-PMAA as a vehicle in the use of chemotherapeutic approaches. Many of the pH-sensitive bonds between a drug and a carrier which are formed from a typical hydrazone linkage were evaluated at pH 5.3 as modeling the extracellular pH environment of cancer cells and at pH 7.4 as modeling the environment of healthy cells.[46] As depicted in Figure 6, free DOX was illustrated the typical release profile at pH 5.3 by reaching 100% release. On the other hand, it was seemed that the cumulative release profile of AuNP-PMAA-Cys-DOX conjugate was more controllable at pH 5.3 according to the free DOX release (Figure 6). Concomitantly, a similar case was also observed at pH 7.4. DOX release from the conjugate at pH 7.4 was about 6.0% up to 72 h. This valuable data demonstrated the potential of AuNP-PMAA-Cys-DOX with a slowly sustained release and usability for a long-time by keeping the formulation at lower temperatures.

Cell Culture. Following the successful characterization steps and defining the release profile of DOX in artificial media modeling the extracellular conditions of cancer cells, in vitro cell culture techniques were used to evaluate the effects of the final DOX conjugate by comparing free DOX and AuNP-PMAA alone with the same concentrations as conjugate. In this manner, cytotoxicity, radiosensitive effect, and cell imaging studies were performed during cell culture experiments. Due to the therapeutic efficacy of DOX and unique radiosensitive activity of AuNPs, a combined modality that is conducted with passive targeting strategy was enabled within bioimaging of HeLa cells within the fluorescence properties of DOX molecule. The related results are given below by discussing the experiments, comparatively.

Cytotoxicity. Before the evaluation of other parameters with HeLa cells as the model cancer cell line in this work, the dose-dependent viability of the cells were determined for AuNP-PMAA, DOX, and AuNP-PMAA-Cys-DOX conjugate for 24 h at 37 °C and 5.0% CO_2 under humidified conditions. Up to date, it is known that AuNPs do not have much toxic effect upon both cancer and healthy cell lines as illustrated in our previous works.[47,48] In this step, AuNP-PMAA structures were initially tested for their influence upon the viability of HeLa cells. Figure 7A represents the effect of polymer-coated AuNP particles on cell viability. It can be clearly said that polymer-coated AuNPs do not exhibit any toxic effect on HeLa cells up to 500 μg/mL particles (84%). As shown in the Figure 7B, the cell viability profile of free DOX is close to AuNP-PMAA-Cys-DOX up to 1.0 μM DOX (equivalent to 50 μg/mL AuNP-PMAA for conjugate). Although DOX was seemed more effective until 5.0 μM, there was a significant decrease between free DOX (47.11%) and AuNP-PMAA-Cys-DOX (25.6%) in the final concentration ($p < 0.001$). It is known that the delivery of free DOX is based on simple diffusion across the cell membrane. Besides, the uptake of many nanocarriers are based on different endoctyic pathways depending on the cell type and the physicochemical properties of nanocarrier.[49] After the uptake of the functional particles, the particles get cleaved in the cells and therapeutic molecules are delivered in the slightly acidic conditions. Since the in vitro DOX release profile presented the similar behavior like other studies, the effect of this profile also can give idea for the cytotoxicity. Moreover, it is always showed that free DOX can release easily under acidic conditions in the cumulative drug release profiles. However, the nanocarrier systems get more effective in the 24 h toxicity tests. In our case, we could observe the effective concentration of the proposed theranostic platform as 5.0 μM DOX concentration. Hence, the constructed DOX conjugate with a pH-sensitive bond may be a good potential in the chemotherapy thanks to its sustained release and having a nontoxic carrier architecture.

Radioactivity. Radiation therapy is one of the most commonly used treatment modality for cancer disease by giving ionizing radiation. It was reported that the effect of ionizing radiation could be enhanced within the addition of high-Z materials, including heavy elements such as gold, *cis*-platin, and so on.[50] Beside this, there may be some difficulties related to the radiotherapy resulting from the acquired radiation resistance. This limitation opens the doorway of the required multiple/combined approaches such as simultaneous applications of drug formulations or treatment modalities like photodynamic therapy/radiotherapy as demonstrated in our previous report.[51] Accordingly, the combination of chemotherapy and radiotherapy by using the enhancers of both modalities, AuNP and DOX were conjugated in a facile and efficient way by creating a pH-sensitive hydrazone linkage. To investigate the radiosensitive effects of AuNP-PMAA-Cys-DOX conjugation, HeLa cells were treated with three different ionizing radiation (2.5, 5.0, and 10 Gray). In addition, free DOX (5.0 μM), AuNP-PMAA, and citrate-coated AuNP (as the same concentration with both AuNP-PMAA and AuNP-PMAA in conjugate) were compared with AuNP-PMAA-Cys-DOX (equivalent to 5.0 μM), comprehensively. As shown in Figure 8, 5.0 Gray of ionizing radiation for AuNP-PMAA-Cys-DOX (27%) demonstrated a significant difference among free DOX (40%), AuNP-PMAA (36.3%), and also citrate-coated AuNPs (46%) by comparing other doses ($p < 0.05$). Meanwhile, DOX was applied to cancer cells in a reported work which supports our findings.[52] In the irradiation of 2.5 and 10 Grays, it is shown that the cell viabilities of the samples ranging from citrate capped AuNPs to AuNP-PMAA-Cys-DOX gave similar results. These results were also compared statistically, however as can be seen from the figure, there is no dramatic change between applied samples for both irradiation doses. Furthermore, the free DOX concentation of 5.0 μM did not present any additional therapeutic effect at 2.5 Gray. The cell viability of that sample is similar to cytotoxicity test. Within the increase of irradiation level, both AuNP-PMAA and DOX created a significant effect according to the control group. As mentioned in introduction part, the radiosensitive effect of AuNPs could demonstrate in this study, clearly.

DOI: 10.1021/acs.biomac.6b00706
Biomacromolecules 2016, 17, 2901−2911

Expectedly, AuNP-PMAA-Cys-DOX particles were able to enhance the therapeutic efficacy comparable to free DOX upon HeLa cells under irradiation of 5 Gray. In other reported studies, DOX was used as a radiosensitizer for HeLa cells and V79 hamster cell line.[53,54] Jagetia and Nayak carried out their research for irradiation effect of DOX by introducing 10 μg/mL (equals to 5.8 μM) DOX to HeLa cells between the range of 0−3.0 Gray irradiation doses.[53] According to this study, increasing irradiation doses enabled a gradual decline in the cell survival compare to control cells without DOX. These results also supports our findings related to the decrease in cell viabilities of free DOX group. As showned in those studies, the high irradiation doses like 10 gray might cause reduced cell viability for control groups without therapeutic molecules. However, samples could significantly show their toxicity upon HeLa cells at 10 Gray, when compare to control group only ($p < 0.001$).

Cell Imaging. As the final study for the synthesized AuNP-PMAA-Cys-DOX, nontoxic concentrations of conjugates were applied to HeLa cells for 2 h to monitor the internalization of DOX conjugates. As can be seen from the Figure 9, DOX in conjugate could easily localize in the nucleus of HeLa cells as free DOX. Beside fluorescent imaging with the unique spectroscopic properties of DOX, phase-contrast images were taken to overlap the images and to show that polymer-coated AuNP conjugate was also effective in monitoring the cells. This capability of the proposed conjugate reveals that it may be a suitable and beneficial candidate as a theranostically engineered nanoparticle.

CONCLUSION

We have examined the functional PMAA-coated AuNPs which were prepared with RAFT polymerization by conjugating with DOX in a pH-sensitive manner. Increasing of the particles sizes and decreased surface charges were evidently demonstrated in the characterization step besides fluorimetric characterization. Furthermore, AuNP-PMAA with 51% DOX binding capacity has shown a sustained drug release in the simulated extracellular matrix conditions by differentiating the pH to prove the pH-sensitive property of AuNP-PMAA-Cys-DOX conjugation. Another considerable influence of the AuNP-PMAA-Cys-DOX was that this novel platform could be used effectively for the treatment of cancer with chemotherapy and radiotherapy modalities when compared only polymer covered AuNPs and DOX. In the final step, we illustrated the capability of this conjugate for cell imaging due to the fluorescence of DOX. Thereby, AuNP-PMAA-Cys-DOX can be a satisfactory theranostic tool in the combined treatment of chemotherapy/radiotherapy and fluorescence imaging.

AUTHOR INFORMATION

Corresponding Authors

*E-mail: r.becer@qmul.ac.uk.
*E-mail: suna.timur@ege.edu.tr.

Notes

The authors declare no competing financial interest.

ACKNOWLEDGMENTS

C.R.B. acknowledges the European Union Horizon2020 (Proposal No. 642083, EURO-SEQUENCES) for funding. F. Baris Barlas (Department of Biochemistry, Ege University), A. Murat Senisik, and H. Armagan Arican from SIFA Hospital (Izmir,Turkey) are acknowledged for their fruitful contributions in radiotherapy studies.

REFERENCES

(1) Doane, T. L.; Burda, C. *Chem. Soc. Rev.* **2012**, *41*, 2885−2911.
(2) Khan, I. U.; Serra, C. A.; Anton, N.; Vandamme, T. *J. Controlled Release* **2013**, *172*, 1065−1074.
(3) Yamashita, F.; Hashida, M. *Adv. Drug Delivery Rev.* **2013**, *65*, 139−147.
(4) Pissuwan, D.; Valenzuela, S. M.; Cortie, M. B. *Trends Biotechnol.* **2006**, *24*, 62−67.
(5) Dutta, P. K.; Dutta, J. *Advances in Polymer Science*; Springer, 2013; Vol. *254*, pp 1−50.
(6) Geyik, C.; Ciftci, M.; Demir, B.; Guler, B.; Ozkaya, A. B.; Gumus, Z. P.; Barlas, F. B.; Odaci Demirkol, D.; Coskunol, H.; Timur, S.; Yagci, Y. *Polym. Chem.* **2015**, *6*, 5470−5477.
(7) Gullotti, E.; Yeo, Y. *Mol. Pharmaceutics* **2009**, *6*, 1041−1051.
(8) Song, W.; Tang, Z.; Li, M.; Lv, S.; Yu, H.; Ma, L.; Zhuang, X.; Huang, Y.; Chen, X. *Macromol. Biosci.* **2012**, *12*, 1375−1383.
(9) Zhang, Y.; Xiao, C.; Li, M.; Chen, J.; Ding, J.; He, C.; Zhuang, X.; Chen, X. *Macromol. Biosci.* **2013**, *13*, 584−594.
(10) Seleci, M.; Ag Seleci, D.; Ciftci, M.; Odaci Demirkol, D.; Stahl, F.; Timur, S.; Scheper, T.; Yagci, Y. *Langmuir* **2015**, *31*, 4542−4551.
(11) Cai, S.; Yang, Q.; Bagby, T. R.; Forrest, M. L. *Adv. Drug Delivery Rev.* **2011**, *63*, 901−908.
(12) Her, S.; Jaffray, D. A.; Allen, C. *Adv. Drug Delivery Rev.* **2015**.
(13) Byrne, J. D.; Betancourt, T.; Brannon-Peppas, L. *Adv. Drug Delivery Rev.* **2008**, *60*, 1615−1626.
(14) Alexis, F.; Pridgen, E.; Molnar, L. K.; Farokhzad, O. C. *Mol. Pharmaceutics* **2008**, *5*, 505−515.
(15) Gu, L.; Mooney, D. J. *Nat. Rev. Cancer* **2015**, *16*, 56−66.
(16) Greco, F.; Vicent, M. J. *Adv. Drug Delivery Rev.* **2009**, *61*, 1203.
(17) Simon, S.; Roy, D.; Schindler, M. *Proc. Natl. Acad. Sci. U. S. A.* **1994**, *91*, 4101.
(18) Liu, J.; Huang, Y.; Kumar, A.; Tan, A.; Jin, S.; Mozhi, A.; Liang, X.-J. *Biotechnol. Adv.* **2014**, *32*, 693−710.
(19) Du, J.-Z.; Mao, C.-Q.; Yuan, Y.-Y.; Yang, X.-Z.; Wang, J. *Biotechnol. Adv.* **2014**, *32*, 789−803.
(20) Shi, J.; Liu, Y.; Wang, L.; Gao, J.; Zhang, J.; Yu, X.; Ma, R.; Liu, R.; Zhang, Z. *Acta Biomater.* **2014**, *10*, 1280−1291.
(21) Chen, X.; Yao, X.; Chen, L.; Chen, X. *Macromol. Biosci.* **2015**, *15*, 1563−1570.
(22) Li, X.; Takashima, M.; Yuba, E.; Harada, A.; Kono, K. *Biomaterials* **2014**, *35*, 6576−6584.
(23) Pan, Y.; Neuss, S.; Leifert, A.; Fischler, M.; Wen, F.; Simon, U.; Schmid, G.; Brandau, W.; Jahnen-Dechent, W. *Small* **2007**, *3*, 1941−1949.
(24) Uboldi, C.; Bonacchi, D.; Lorenzi, G.; Hermanns, M. I.; Pohl, C.; Baldi, G.; Unger, R. E.; Kirkpatrick, C. J. *Part. Fibre Toxicol.* **2009**, *6* (18), 1−12.
(25) Niidome, T.; Yamagata, M.; Okamoto, Y.; Akiyama, Y.; Takahashi, H.; Kawano, T.; Katayama, Y.; Niidome, Y. *J. Controlled Release* **2006**, *114*, 343−347.
(26) Hauck, T. S.; Ghazani, A. A.; Chan, W. C. W. *Small* **2008**, *4*, 153−159.
(27) Choi, C. H. J.; Alabi, C. A.; Webster, P.; Davis, M. E. *Proc. Natl. Acad. Sci. U. S. A.* **2010**, *107*, 1235−1240.
(28) Cheng, D.; Han, W.; Yang, K.; Song, Y.; Jiang, M.; Song, E. *Talanta* **2014**, *130*, 408−414.
(29) Wu, Y.; Zuo, F.; Lin, Y.; Zhou, Y.; Zheng, Z.; Ding, X. *J. Macromol. Sci., Part A: Pure Appl.Chem.* **2014**, *51*, 441−446.
(30) Dhumale, V. A.; Gangwar, R. K.; Datar, S. S.; Sharma, R. B. *Mater. Express* **2012**, *2*, 311−318.
(31) Li, L.; Nafiujjaman, N.; Lee, Y. K.; Huh, K. M. *J. Controlled Release* **2013**, *171*, 241−250.
(32) Muddineti, O. S.; Ghosh, B.; Biswas, S. *Int. J. Pharm.* **2015**, *484*, 252−267.
(33) Jiao, P.; Zhou, H.; Chen, X.; Yan, L. *Curr. Med. Chem.* **2011**, *18*, 2086−2102.

DOI: 10.1021/acs.biomac.6b00706
Biomacromolecules 2016, 17, 2901−2911

(34) Du, W.; Yuan, Y.; Wang, L.; Cui, Y.; Wang, H.; Xu, H.; Liang, G. *Bioconjugate Chem.* **2015**, *26*, 2571−2578.
(35) Shanthi, K.; Vimala, K.; Gopi, D.; Kannan, S. *RSC Adv.* **2015**, *5*, 44998−45014.
(36) He, C.; Hu, Y.; Yin, L.; Tang, C.; Yin, C. *Biomaterials* **2010**, *31*, 3657−3666.
(37) Alexis, F.; Pridgen, E.; Molnar, L. K.; Farokhzad, O. C. *Mol. Pharmaceutics* **2008**, *5*, 505−515.
(38) Aggarwal, P.; Hall, J. B.; McLeland, C. B.; Dobrovolskaia, M. A.; McNeil, S. E. *Adv. Drug Delivery Rev.* **2009**, *61*, 428−437.
(39) Rück-Braun, K.; Petersen, M. A.; Michalik, F.; Hebert, A.; Przyrembel, D.; Weber, C.; Ahmed, S. A.; Kowarik, S.; Weinelt, M. *Langmuir* **2013**, *29*, 11758−11769.
(40) Ma, W.; Xu, S.; Li, J.; Guo, J.; Lin, Y.; Wang, C. *J. Polym. Sci., Part A: Polym. Chem.* **2011**, *49*, 2725−2733.
(41) Mattevi, C.; Hofmann, S.; Cantoro, M.; Ferrari, A. C.; Robertson, J.; Castellarin-Cudia, C.; Dolafi, S.; Goldoni, A.; Cepek, C. *Phys. E* **2008**, *40*, 2238−2242.
(42) Beverly, S.; Seal, S.; Hong, S. *J. Vac. Sci. Technol., A* **2000**, *18*, 1107−1113.
(43) Huang, Y.-L.; Baji, A.; Tien, H.-W.; Yang, Y.-K.; Yang, S.-Y.; Ma, C-C.M.; Liu, H.-Y.; Mai, Y.-W.; Wang, N.-H. *Nanotechnology* **2011**, *22*, 1−7.
(44) Casaletto, M. P.; Kaciulis, S.; Mattogno, G.; Mezzi, A.; Ambrosio, L.; Branda, F. *Surf. Interface Anal.* **2002**, *34*, 45−49.
(45) Wong, L.; Kavallaris, M.; Bulmus, V. *Polym. Chem.* **2011**, *2*, 385−393.
(46) Strambi, A.; De Milito, A. *Tumor Cell Metabolism*; Springer, 2015; pp 173−196.
(47) Unak, G.; Ozkaya, F.; Medine, E. I.; Kozgus, O.; Sakarya, S.; Bekis, R.; Unak, P.; Timur, S. *Colloids Surf., B* **2012**, *90*, 217−226.
(48) Demir, B.; Barlas, F. B.; Guler, E.; Gumus, P. Z.; Can, M.; Yavuz, M.; Coskunol, H.; Timur, S. *RSC Adv.* **2014**, *4*, 34687−34695.
(49) Shuai, X.; Ai, H.; Nasongkla, N.; Kim, S.; Gao, J. *J. Controlled Release* **2004**, *98*, 415−426.
(50) Cooper, D. R.; Bekah, D.; Nadeau, J. L. *Front. Chem.* **2014**, *2* (86), 1−13.
(51) Barlas, F. B.; Demir, B.; Guler, E.; Senisik, A. M.; Arican, H. A.; Unak, P.; Timur, S. *RSC Adv.* **2016**, *6*, 30217−30225.
(52) Xu, W. H.; Han, M.; Dong, Q.; Fu, Z. X.; Diao, Y. Y.; Liu, H.; Xu, J.; Jiang, H. L.; Zhang, S. Z.; Zheng, S.; Gao, J. Q.; Wei, Q. C. *Int. J. Nanomed.* **2012**, *7*, 2661−2671.
(53) Jagetia, G. C.; Nayak, V. *Strahlenther. Onkol.* **2000**, *176*, 422−428.
(54) Bonner, J. A.; Lawrence, L. A. *Int. J. Radiat. Biol.* **1990**, *57*, 55−64.

DOI: 10.1021/acs.biomac.6b00706
Biomacromolecules 2016, 17, 2901−2911